Accepted Manuscript – Final publication in Acta Materialia 183, 242-248 (2020)

Intrinsic Toughness of the Bulk-Metallic Glass Vitreloy 105 Measured Using Micro-Cantilever Beams

Daniel Sorensen*[a, b], Eric Hintsala[c], Jesse Pischlar[a], Joseph Stevick[d], Bernard Li[a], Daniel Kiener[e], Jason C. Myers[f], Hui Jin[a], Jia Liu[a], Douglas Stauffer[c], Antonio. J. Ramirez[b] and Robert O. Ritchie[g]

[a]Medtronic PLC, Minneapolis, MN 55432, USA

[b]Department of Materials Science and Engineering, Ohio State University, Columbus, OH 43221, USA

[c]Hysitron Inc., Eden Prairie, MN 55344, USA

[d]Liquidmetal Technologies, Rancho Santa Margarita, CA 92688, USA

[e]Department of Materials Physics, Montanuniversität Leoben, Leoben, Austria

[f]University of Minnesota Characterization Facility, Minneapolis, MN 55455, USA

[g]Materials Sciences Division, Lawrence Berkeley National Laboratory, and Department of Materials Science and Engineering, University of California, Berkeley, CA 94720, USA

*To whom all correspondence should be addressed.

Abstract

Bulk-metallic glasses (BMGs) are a class of structural materials with many attractive mechanical properties such as the ability to be processed into parts with fine features, dimensional precision, and repeatability; however, their fracture behavior is complex and size-dependent. Previous work has shown that BMGs can display strong size effects on toughness, where multiple mechanisms on different length-scales , *e.g.*, crack bridging and bifurication, shear band spacing and length, can significantly affect the properies. This length-scale dependence on the fracture toughness has importance not only for advancing the understanding of fracture processes in these materials, but also for the potential future applications of BMGs, such as for microdevices. Here, using *in situ* scanning electron microscopy (SEM), we report on notched micro-cantilever bending experiments to address the lack of data regarding fracture properties of BMGs at the microscale. Sudden catastrophic propagation of shear bands resulted in failure for these specimens at stress intensities much lower than the bulk material which is may be due to a lack of extrinsic toughening mechanisms at these dimensions. This is explored further with post mortem SEM and transmission electron microscopy (TEM) analysis of the fractured beams while the fracture toughness results are verified using finite element modeling. The excellent agreement between model and micro cantilever beam bending experiments suggests that the intrinsic fracture toughness of Vitreloy 105 is being reported for the first time.

Keywords: bulk-metallic glasses, fracture toughness; micro-cantilever testing, length-scale dependence

Published version available at http://dx.doi.org/10.1016/j.actamat.2019.11.021

1. Introduction

Bulk-metallic glasses (BMGs) are a relatively new class of engineering materials with many desireable properties such as high elastic limit, low elastic modulus, corrosion resistance, and the ability to be formed using injection molding into near-net shapes [1]. One of the largest issues limiting the widespread use of bulk metallic glasses is the inconsistency in the fracture toughness which has been shown to vary with part dimensions [2,3], material processing, and composition [4,5]. While many researchers have related such variations in fracture toughness on milli- to macro length-scale parts [6,7] to deformation and shear band formation at the sub-micron and nano scales [8-10], the fracture and fatigue behavior of bulk metallic glasses is still an active area of research.

The ability to fabricate bulk metallic glasses on the thickness scale of tens of micrometers creates numerous possible engineering applications that include MEMS devices [11], foils for sensors [12], leaf valves [13], springs [14], and hinges [15]. However, to the authors' knowledge, no data on fracture properties exists at the micrometer length-scale for BMGs, which is required for any eventual commercial development of engineered components.

Here we report on the failure analysis and fracture toughness of micron-scale specimens of a commercially available Zr-based bulk-metallic glass, Vitreloy 105, using *in situ* micro cantilever beam bending, *post mortem* SEM fractograhy, TEM analysis and finite element modeling. Comparison of our results to nanoscale and millimeter scale studies is utilized to achieve a more comprehensive understanding of length-scale effects on the toughness and mechanical performance of these amorphous materials.

2. Experimental

The material used for this experiment was a 0.9 mm thick plate of Zr-based bulk-metallic glass (Vitreloy 105) with composition in wt.% of Zr-14.8Cu-11.3Ni-3.6Al-3.2Ti-0.047Be-0.013Si, measured by inductively coupled plasma-optical emission spectroscopy (ICP-OES). Sections of the plate were cut to 100 mm^2 samples by electrical discharge machining (EDM) and the part surfaces were ground and prepared to a 50 nm final polish using an Allied MultiPrep polishing system. The amorphous structure of the samples was confirmed using x-ray diffraction. The microbeams were fabricated by Ga^+ ions at 30 kV using an FEI Scios field emission gun scanning electron microscope/focused ion beam (FEGSEM/FIB). Initial shape profiling was performed at probe currents starting at 65 nA progressively reducing down to 1 nA and all surfaces were final polished using a 100 pA probe current. The side cuts were made using a 2° over tilt to minimize taper. The notches were fabricated using an ion beam accelerating voltage of 5 kV, probe current of 48 pA, and Z depth of 500 nm using a standard line pattern. The larger 5 kV probe created a line with a narrow parabolic shape and opening at the surface making material re-deposition less of an issue while achieving radii of curvature at the notch root on the order of 25 nm. The notch depth was targeted to be on the order of 1.5 µm to achieve notch depth to thickness (*a/W*) ratios of approximately 0.45. Fig. 1 shows a representative beam with critical dimensions labeled.

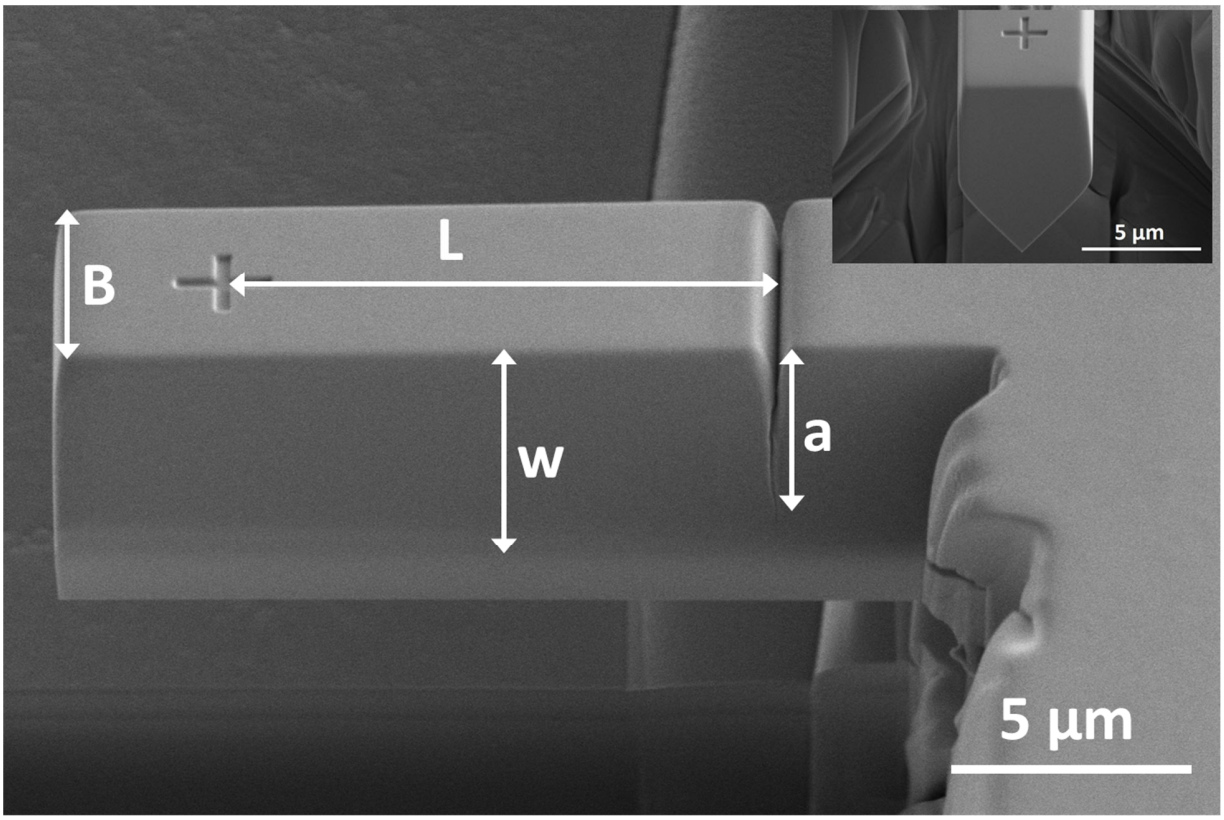

Fig. 1. SEM image of a representative Vitreloy 105 micro-cantiliever beam with important dimensions labeled and end view shown in the inset.

All testing was performed with a Hysitron PI-85 PicoIndenter *in situ* in a FEI Versa field emission gun (FEG) SEM/FIB operating at 20 kV. All beams (n=10) were loaded using a conical diamond milled to a 2 µm flat punch in displacement control mode at 20 nm·sec^{-1}. Although fatigue and crack propagation of the Vitreloy 1 and 106a alloys have been reported to be sensitive to test environments ranging from ambient air to inert gasses [16,17], similar studies on Vitreloy 105 have shown the fatigue and fracture properties to be essentially independent of test environment [18]. This gives confidence that fracture toughness data collected inside the vacuum chamber of a FEG SEM over relatively short time scales are representative of samples tested in ambient conditions. Fracture surfaces of the failed samples were analyzed *post mortem* using an FEI Scios SEM operating at 5 keV. Samples for transmission electron microscopy were lifted out from fractured beams using an FEI Scios FEGSEM/FIB fitted with an EasyLift system, prepared using a 2° overtilt for all polishing steps, and final polished using a 5 keV beam. TEM analysis was performed using an FEI Tecnai G^2 F30 operating at 300 keV.

Finite element analysis (FEA) was performed using Abaqus 6.14 commercial software. The beam model was discretized into second order hex 3D elements (Abaqus element type C3D20R). The mesh around the notch was highly refined to capture the stress gradient near the tip. J integral output with eighteen contours was requested and its convergence was monitored. The material constitutive law is assumed be to classical metal plasticity with isotropic hardening. Displacement control was applied to a reference point coupled with a small region on the beam, mimicking the contact between the indenter and the beam. To obtain the energy release rate, J integral method with 10 contours was applied in the model.

The convergence of the contour integrals was monitored, and the converged value was readily taken as the energy release rate.

Figure 3 shows the force-displacement curves for 10 tested samples, superimposed by FEA results. In the FEA model, the geometry was built using the measured mean dimensions of the 10 tested samples. The linear elastic constants (Young's modulus and Poisson's ration) were determined by nano-indentation, as mentioned above. Excellent agreement can be seen for the linear regime, indicating that FEA model predicts faithfully the bending stiffness of the beam. Note that the material strain hardening inputs were tuned (1.95GPa, 0; 3.25GPa, 0.005) to capture the plastic behavior.

As a secondary check of the calculated *J*, we also compare with the FEA predicted value, obtained from the center plane of the beam. At displacement of 2900 nm, energy release rate results from the *J* integral analysis were found to converge at 0.91 N/mm which agrees with our experimentally measured values of 0.935 N/mm. The strain energy release rates *G* and *J* were used to calculate K_J from the FEA model which was found to be 9.55 MPa·m$^{1/2}$, *i.e.*, in excellent agreement with the experimental results. Furthermore, the Von Mises stress contours (Fig. 4 b) in the deformed model agreed with the locations of shear band formation, plastic-zone size, and final fracture. Results of contour integral analysis showing convergence are presented in Fig. 3 c.

3. Results and Discussion

The micro cantilevers all failed catastrophically after limited plastic deformation. A representative montage of images from an *in situ* experiment and their locations on the corresponding load-displacement curve are shown in Fig. 2.

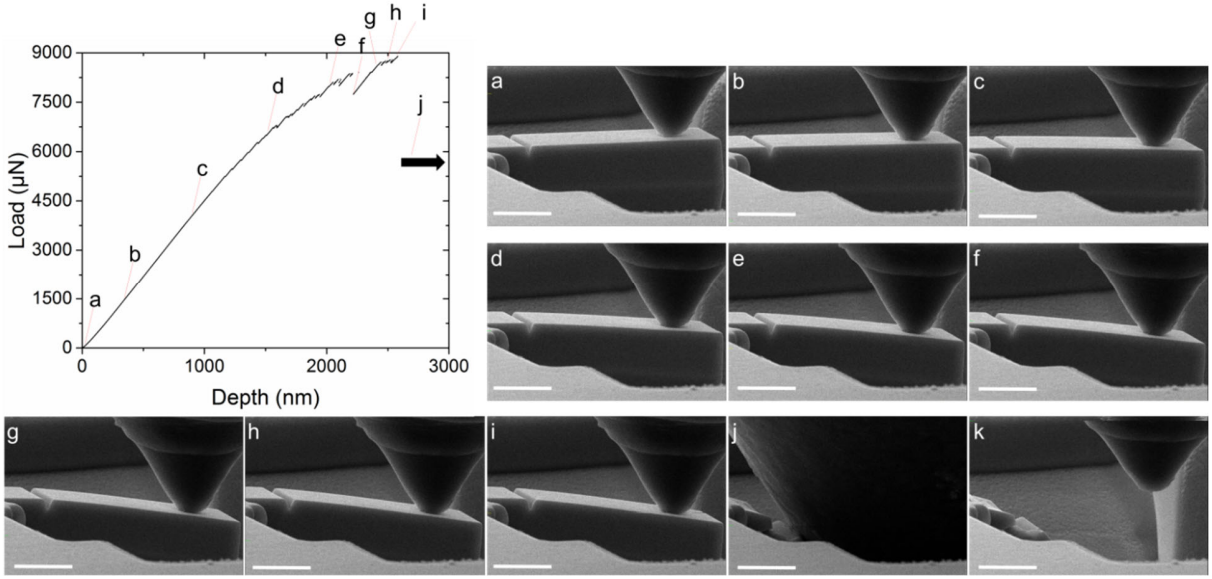

Fig. 2. – Screen capture montage showing deformation of a representative Vitreloy 105 beam at several points on the load-displacement curve. The load drops (serrations) were confirmed to be the result of shear band propagation events during *post mortem* analysis. Scale bar signifies a length of 5 μm.

Three distinct deformation regimes can be seen in the loading curves: elastic bending, limited plastic flow indicated by serrations in the load-displacement curve, and catastrophic failure. The serrated plastic flow was the result of shear band formation which was confirmed by *post mortem* analysis, constant loading stiffness prior to and immediately following the load drop, observation of opening of the notch flanks, and slight blunting of the crack tip. This type of shear band initiation was also found in previous research utilizing micro indentation, nanoindentation, and nano pillar compression testing [19-21]. The combined results for all micro cantilever beam bending experiments, shown overlaid in Fig. 3a, display the same characteristics as Fig. 2, with a slight shift in load at the same displacement correlated with the notch length.

To evaluate the fracture toughness from these data, first it is important to establish the regime that these tests are being conducted in. A linear-elastic fracture mechanics (LEFM) analysis was initially utilized to calculate the provisional critical stress intensity, K_Q, for the purposes of evaluating the plastic-zone size in relation to the specimen dimensions. To achieve this, the classic elastic cantilever solution (Eq. 1a,b), similar to that used by Zhao *et al.* [22] and Di Maio and Roberts [23], was employed to compute the stress intensities as a function of load, crack size and sample dimensions. The results can be found in Table I, along with estimates of the plastic-zone size, $r_y \sim 1/2\pi (K_Q/\sigma_y)^2$, and statistical sampling volume (*SSV*), calculated using the yield stress, σ_y, and elastic modulus, *E*, as determined by nanoindentation (1.95 GPa and 85.6 GPa, respectively):

$$K_Q = \sigma_c \sqrt{\pi a} f\left(\frac{a}{W}\right), \qquad (1)$$

where

$$f\left(\frac{a}{W}\right) = 1.85 - 3.38\left(\frac{a}{W}\right) + 13.24\left(\frac{a}{W}\right)^2 - 23.26\left(\frac{a}{W}\right)^3 + 16.8\left(\frac{a}{W}\right)^4. \qquad (2)$$

Table I. Measured and computed average values with standard deviations of the provisional linear elastic fracture toughness, K_Q, plastic-zone size, r_y, and the nonlinear-elastic $J_{c,exp}$ fracture toughness and the critical stress intensity $K_{Jc,exp}$, back-calculated from this *J* value.

K_Q (MPa.m$^{1/2}$)	**r_y** (μm)	**r_y/B**	**r_y/w**	**SSV** (μm)	**$Jc_{,exp}$** (J/m^2)	**$K_{Jc,exp}$** (MPa.m$^{1/2}$)	**$K_{Jc,FEA}$** (MPa.m$^{1/2}$)
9.77±1.1	4.04±0.92	0.59±0.13	1.09±0.29	0.58±.13	935.3±178.3	9.63±0.94	9.55

It can be observed from Table I that the measured linear-elastic fracture toughness was found to be K_Q = 9.77 MPa.m^{½}; using this value, the estimate of the plastic-zone size can be seen to exceed one tenth of both the beam width and the beam thickness, which indicates that the specimen dimensions did not meet the ASTM Standard 1820 [25] for Fracture Toughness Testing with respect to both the *K*-field dominance of the crack-tip stress and displacement fields (small-scale yielding) and plane-strain constraint, respectively. Thus, the calculated values could not be strictly labeled as the fracture toughness K_c or plane-strain fracture toughness $K_{Ic,}$ in view of the small size of the samples. Considering this, we employed a nonlinear-elastic fracture mechanics methodology to determine the critical value of

the *J*-integral at fracture, J_{exp}, using measurements of the total work of fracture (involving elastic and plastic contributions), A_{cur}, and the specimen and crack size dimensions, as per ASTM Standard 1820 [25]. Specifically, this was calculated by integrating area under the load-depth curves using Origin software to determine the mechanical work and then normalizing by the failed ligament cross-section, according to Eq. 3:

$$J = \frac{2A_{cur}}{(W-a)*B+\frac{B^2}{4}} \quad , \qquad (3)$$

where *W* is the beam width and *B* the beam thickness. The calculated *J* value at fracture, $J_{Ic,exp}$, was found to be ~935 J/m^2; the validity for this value, as per ASTM Standard 1820 in terms of the existence of *J*-dominant crack-tip fields, can be achieved if both *B* and (*W*-*a*) > 10 J_{exp}/σ_{flow}, where σ_{flow} is the average calculated bending stress of the cantilevers tested (3076 MPa). A stress-intensity based fracture toughness, $K_{J,exp}$, was then be back-calculated from the critical $J_{Ic,exp}$ value at fracture value, using the standard mode I *K*-*J* equivalence, *i.e.*, $J = K^2/E'$, where the Young's modulus value in plane strain is given in terms of Poisson's ratio ν as $E' = E/(1-\nu^2)$. The resulting *J*-based fracture toughness, $K_{Jc,exp}$, was found to be 9.63 MPa.m^{½}.

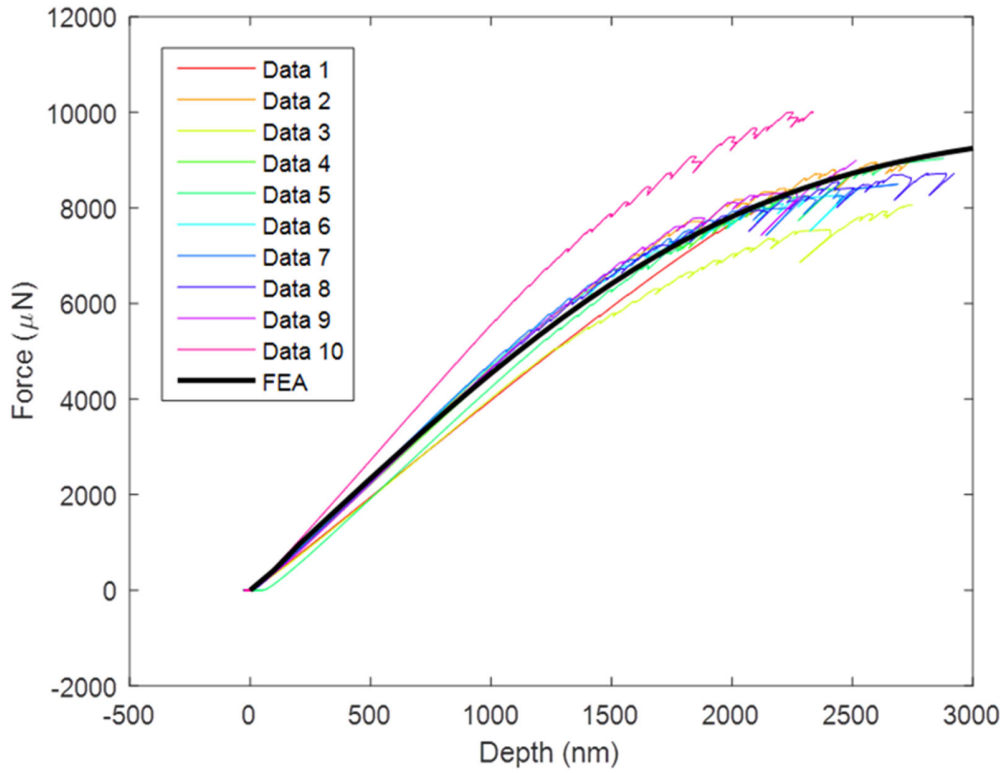

Fig. 3. Plots of load-displacement curves for all 10 micro-cantilevers fractured in this study with overlaid FEA result.

The good agreement between the various experimental and numerical estimates of the fracture toughness of this metallic glass at the micron-scale, namely a slightly invalid LEFM experimental K_Q value of 9.77 MPa.m^{½}, a valid, plane-strain K_{Jc} value (determined experimentally using *J*-based measurements) of 8.91 MPa.m^{½}, and a numerically determined value (based on energy-release rates) of 9.4 MPa·m$^{1/2}$,

supports the conclusion that the fracture toughness of these specimens has been realistically determined to be on the order of 9 MPa·m$^{1/2}$ at the micron-scale. This is to be contrasted with the toughness values reported in the literature for millimeter-sized samples of Vitreloy 1 [6,7] and Vitreloy 105 [2,4], where K_{Ic} values have been reported to be between 20-100 MPa·m$^{1/2}$, *i.e.*, between 2 and 10 times higher. Significant issues with size-effects on the toughness of BMGs have been reported for measurements on the millimeter scale [2] and on shear band formation down to hundreds of nanometers [8,9,27,28]. In general, smaller metallic glass samples were found to have relatively higher toughness due to a loss of plane-strain confinement as the sample size decreased to around 2 mm [2]. In fact, early millimeter-scale fracture tests resulted in what were considered surprisingly high fracture toughness values when compared against an estimate using the Taylor instability [6], which resulted in a value of 13 MPa·m$^{1/2}$, which approaches our experimental measurements here. Additionally, there has been concern over the extent of validity of *J*-based analysis for BMGs [2] due to their limited strain hardening [26], which would act to restrict the extent of the HRR-singularity of stress and displacement fields at the crack tip upon which the uniqueness of the *J*-field is based [29,30]. However, we do not believe that this is a major problem with the current values due to the similarity of the linear-elastic *K*-based and nonlinear-elastic *J*-based toughness estimates and their agreement with the numerically derived value. Since the results presented here represent an crack-initiation toughness only, *i.e.*, fracture occurred catastrophically with crack instability simultaneous with initiation, there no evidence of stable cracking or crack-resistance R-curve behavior, which often is the basis of extrinsic toughening mechanisms*, such as the crack-bridging and deflection phenomena that clearly affects some of the higher values reported for the bulk scale [2]. Indeed, *post mortem* SEM and FEA analysis, shown in Fig. 4, demonstrate clearly that fracture occurred catastrophically in a volume approaching the thickness of the beam.

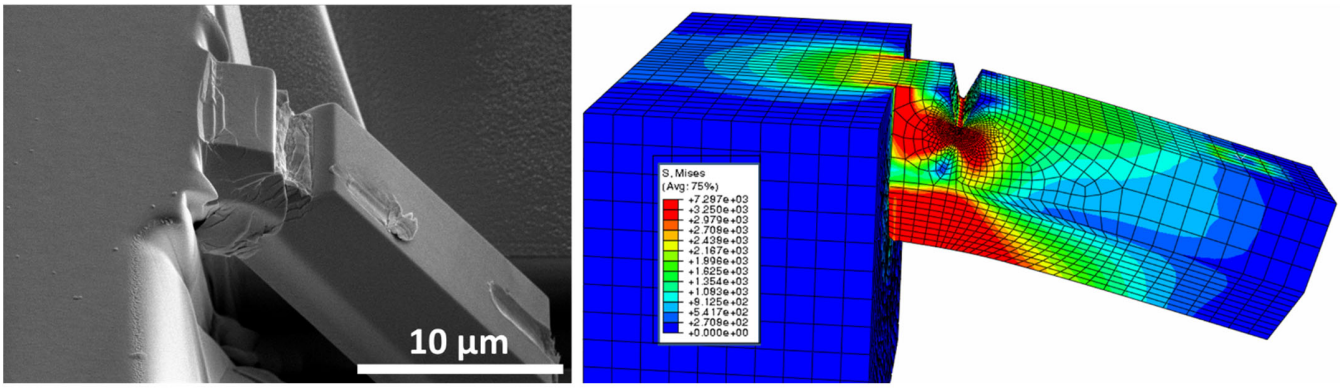

Fig. 4. (a) Fractograph showing a profile of a representative Vitreloy 105 beam following a catastrophic failure compared to (b) FEA model of a deformed Vitreloy 105 beam following a 2900 nm displacement at the end of the beam. Note the locations of the beam where shear banding and a large plastic zone were experimentally observed, in areas with the highest Von Mises stresses as predicted in the model in units of MPa.

* Fracture resistance can be considered as a mutual competition between two classes of toughening mechanisms: intrinsic mechanisms, which resist microstructural damage ahead of the crack tip and are motivated primarily by plasticity, and extrinsic mechanisms, which operate at, or in the wake of, the crack tip to inhibit fracture by "shielding" the crack from the applied driving force [31]. Whereas intrinsic toughening mechanisms are effective in inhibiting both the initiation and growth of cracks, extrinsic toughening mechanisms, such as crack bridging and crack deflection, are only effective in inhibiting crack growth.

The fracture surface morphology of failed cantilevers indicate areas of local melting from shear band formation, similar to that reported in ref. [19], and crack propagation involving classic brittle fracture. The shear band spacing was on the order of 500 nm and followed the trend reported by Conner *et al.* where bending experiments of Zr-based metallic glass showed shear band spacing decreased as sample size decreased [32]. Liu *et al*. also reported a shear band spacing/sample geometry relationship resulting in brittle fracture when the sample geometry is decreased [33,34]. These observations agree with our *post mortem* analysis of primary shear band spacing seen in Fig. 5a. Lastly, transmission electron microscope (TEM) samples prepared from failed beams showed no signs of crystallization at the notch root or shear bands that may have impacted the toughness measurements. The TEM/selected area diffraction (SAD) analysis showed the beam remained amorphous at the notch tip after ion beam fabrication and after final fracture.

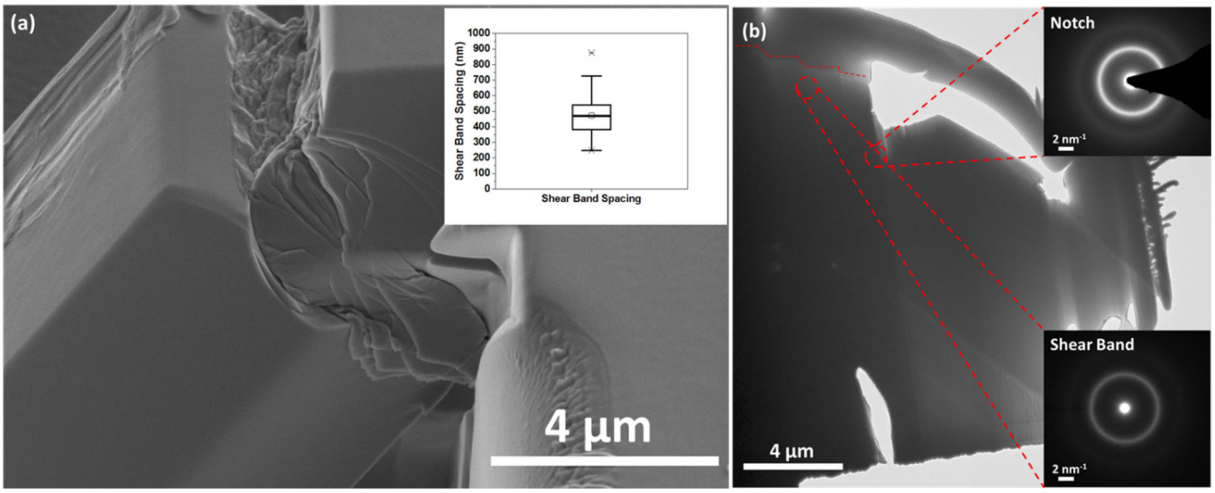

Fig. 5. (a) High magnification fractograph showing shear banding and catastrophic brittle fracture in detail. Inset boxplot showing the shear band spacing distribution for all pentagonal beams tested in this study. (b) Transmission electron micrograph with inset selected area diffraction patterns showing a lack of crystallization caused by FIB milling at the notch tip or local melting during shear band formation. The surface steps from the shear banding are highlighted by a dotted line.

From an engineering standpoint, these results, that the micron-scale fracture toughness of bulk-metallic glasses, may be up to an order of magnitude lower than corresponding values measured at the millimeter-scale, are important because components made from BMGs containing micron-scale features may not have the toughening observed in larger samples. This markedly lower micron-scale toughness should be considered when designing small scale components with small scale features, thin films, or MEMS devices using BMGs.

4. Conclusions

The fracture properties of micron-scale samples of Vitreloy 105 bulk-metallic glass show a size effect with a markedly different fracture toughness from that of mill- to macro-scale specimens, where high

toughness and extrinsic toughening behavior have been observed. The simplified analyses showed an average fracture toughness at crack initiation/instability ranged from 9.77 (K_Q LEFM measurements) to 9.63 (valid *J*-based measurements) MPa·m$^{1/2}$ and 9.4 MPa·m$^{1/2}$ (FEA-based energy-release rate simulation), values which are between a factor of 2 to 10 times lower than measurements reported for this glass in the literature for larger-scale samples. Experimental observations and plastic-zone size calculations suggest the low fracture toughness is related to the cantilever dimensions being on the same order as the plastic zone, resulting in small amounts of shear banding followed by catastrophic failure, with no evidence of extrinsic toughening and resistance-curve behavior. The findings presented in this study are critical components for the further understanding of the metallic glass fracture toughness size effect phenomenon.

Acknowledgements

The authors would like to acknowledge the Medtronic Restorative Therapies Group leadership for financial support of this research. DS would also like to thank Mr. Brandon Van Leer and Dr. Jan Ringnalda of Thermo Fischer Scientific for helpful sample preparation advice, Mr. Peter Yurek of Medtronic for performing the x-ray diffraction experiment, Mr. Brian Leigh of Medtronic for performing the ICP-OES analysis, and Ms. Margaret Flury of Medtronic for careful proofreading of this manuscript. Parts of this work were carried out in the Characterization Facility, University of Minnesota, which receives partial support from NSF through the MRSEC program. ROR was supported by the Office of Science, Office of Basic Energy Sciences, Materials Sciences and Engineering Division, under contract no. DE-AC02-05CH11231.

References

[1] C. Suryanarayana and A. Inoue, *Bulk Metallic Glasses*. CRC Press, 2011.

[2] B. Gludovatz, S. E. Naleway, R. O. Ritchie, and J. J. Kruzic, "Size-dependent fracture toughness of bulk metallic glasses," *Acta Materialia,* vol. 70, pp. 198-207, 5/15/ 2014.

[3] B. Gludovatz, D. Granata, K. V. S. Thurston, J. F. Löffler, and R. O. Ritchie, "On the understanding of the effects of sample size on the variability in fracture toughness of bulk metallic glasses," *Acta Materialia,* vol. 126, pp. 494-506, 3// 2017.

[4] W. Chen *et al.*, "Processing effects on fracture toughness of metallic glasses," *Scripta Materialia,* vol. 130, pp. 152-156, 3/15/ 2017.

[5] V. Schnabel *et al.*, "Electronic hybridisation implications for the damage-tolerance of thin film metallic glasses," *Scientific Reports,* Article vol. 6, p. 36556, 11/07/online 2016.

[6] C. J. Gilbert, R. O. Ritchie, and W. L. Johnson, "Fracture toughness and fatigue-crack propagation in a Zr–Ti–Ni–Cu–Be bulk metallic glass," *Applied Physics Letters,* vol. 71, no. 4, pp. 476-478, 1997/07/28 1997.

[7] C. J. Gilbert, V. Schroeder, and R. O. Ritchie, "Mechanisms for fracture and fatigue-crack propagation in a bulk metallic glass," *Metallurgical and Materials Transactions A,* vol. 30, no. 7, pp. 1739-1753, 1999.

[8] O. V. Kuzmin, Y. T. Pei, C. Q. Chen, and J. T. M. De Hosson, "Intrinsic and extrinsic size effects in the deformation of metallic glass nanopillars," *Acta Materialia,* vol. 60, no. 3, pp. 889-898, 2// 2012.

[9] D. Jang, C. T. Gross, and J. R. Greer, "Effects of size on the strength and deformation mechanism in Zr-based metallic glasses," *International Journal of Plasticity,* vol. 27, no. 6, pp. 858-867, 6// 2011.

[10] C. Q. Chen, Y. T. Pei, and J. T. M. De Hosson, "Effects of size on the mechanical response of metallic glasses investigated through in situ TEM bending and compression experiments," *Acta Materialia,* vol. 58, no. 1, pp. 189-200, 1// 2010.

[11] T. Fukushige, S. Hata, and A. Shimokohbe, "A MEMS conical spring actuator array," *Journal of Microelectromechanical Systems,* vol. 14, no. 2, pp. 243-253, 2005.

[12] Z. Wang *et al.*, "Magnetoelectric effect in crystallographically textured BaTiO3 films deposited on ferromagnetic metallic glass foils," *Journal of Applied Physics,* vol. 109, no. 3, p. 034102, 2011/02/01 2011.

[13] K. Richter, "Amorphous metal alloy medical devices," ed: Google Patents, 2011.

[14] J. F. Löffler, "Bulk metallic glasses," *Intermetallics,* vol. 11, no. 6, pp. 529-540, 6// 2003.

[15] J. H. Tregilgas, "Amorphous Titanium Aluminide Hinge," vol. 162, ed. Adv Mater Proc, 2004, pp. 40-41.

[16] S. L. Philo and J. J. Kruzic, "Fatigue crack growth behavior of a Zr–Ti–Cu–Ni–Be bulk metallic glass: Role of ambient air environment," *Scripta Materialia,* vol. 62, no. 7, pp. 473-476, 4// 2010.

[17] S. L. Philo, J. Heinrich, I. Gallino, R. Busch, and J. J. Kruzic, "Fatigue crack growth behavior of a Zr58.5Cu15.6Ni12.8Al10.3Nb2.8 bulk metallic glass-forming alloy," *Scripta Materialia,* vol. 64, no. 4, pp. 359-362, 2// 2011.

[18] S. E. Naleway, R. B. Greene, B. Gludovatz, N. K. N. Dave, R. O. Ritchie, and J. J. Kruzic, "A Highly Fatigue-Resistant Zr-Based Bulk Metallic Glass," *Metallurgical & Materials Transactions. Part A,* Article vol. 44, no. 12, pp. 5688-5693, 2013.

[19] W. J. Wright, R. B. Schwarz, and W. D. Nix, "Localized heating during serrated plastic flow in bulk metallic glasses," *Materials Science and Engineering: A,* vol. 319–321, pp. 229-232, 12// 2001.

[20] C. A. Schuh and T. G. Nieh, "A nanoindentation study of serrated flow in bulk metallic glasses," *Acta Materialia,* vol. 51, no. 1, pp. 87-99, 1/8/ 2003.

[21] W. Wright, nbsp, J, R. Saha, W. Nix, and D, "Deformation Mechanisms of the Zr40Ti14Ni10Cu12Be24 Bulk Metallic Glass," *MATERIALS TRANSACTIONS,* vol. 42, no. 4, pp. 642-649, 2001.

[22] X. Zhao, R. M. Langford, J. Tan, and P. Xiao, "Mechanical properties of SiC coatings on spherical particles measured using the micro-beam method," *Scripta Materialia,* vol. 59, no. 1, pp. 39-42, 7// 2008.

[23] D. Di Maio and S. G. Roberts, "Measuring fracture toughness of coatings using focused-ion-beam-machined microbeams," *Journal of Materials Research,* vol. 20, no. 2, pp. 299-302, 2005/002/001 2005.

[24] Y. Murakami, *Stress intensity factors handbook. 1 (1987)* (Stress Intensity Factors Handbook). Elsevier Science Limited, 1987.

[25] ASTM E1820-17a, Standard Test Method for Measurement of Fracture Toughness, ASTM International, West Conshohocken, PA, 2017

[26] H. Bei, S. Xie, and E. P. George, "Softening Caused by Profuse Shear Banding in a Bulk Metallic Glass," *Physical Review Letters,* vol. 96, no. 10, p. 105503, 03/16/ 2006.

[27] A. Bharathula, S.-W. Lee, W. J. Wright, and K. M. Flores, "Compression testing of metallic glass at small length scales: Effects on deformation mode and stability," *Acta Materialia,* vol. 58, no. 17, pp. 5789-5796, 10// 2010.

[28] B. Chen, T. L. Shi, M. Li, F. Yang, F. Yan, and G. L. Liao, "Laser welding of annealed Zr55Cu30Ni5Al10 bulk metallic glass," *Intermetallics,* vol. 46, pp. 111-117, 3// 2014.

[29] J. W. Hutchinson, "Singular behavior at the end of a tensile crack in a hardening material," *Journal of the Mechanics and Physics of Solids*, vol. 16, pp. 13-31, 1968.

[30] J. R. Rice and G. F. Rosengren, "Plane strain deformation near a crack tip in a power-law hardening material," *Journal of the Mechanics and Physics of Solids*, vol. 16, pp. 1-12, 1968.

[31] R. O. Ritchie, "The conflicts between strength and toughness," *Nature Materials*, vol. 10, pp. 817-822, 2011.

[32] R. D. Conner, Y. Li, W. D. Nix, and W. L. Johnson, "Shear band spacing under bending of Zr-based metallic glass plates," *Acta Materialia,* vol. 52, no. 8, pp. 2429-2434, 5/3/ 2004.

[33] F. X. Liu *et al.*, "Specimen-geometry effects on mechanical behavior of metallic glasses," *Intermetallics,* vol. 14, no. 8–9, pp. 1014-1018, 8// 2006.

[34] J.-Y. Suh, D. R. Conner, P. C. Kim, M. Demetriou, and W. Johnson, "Plastic Zone Formation and Fracture of Zr-based Bulk Metallic Glasses," presented at the Society for Experimental Mechanics Annual Conference Albuquerque New Mexico USA, 2009.

Appendix

The stress on a micro-cantilever beam during a point loaded bending experiment is shown in Eq. A1 where F is the applied load, L is the distance between the notch and point where the load was applied, y is the vertical distance between the top of the beam and the neutral plane, and I is the moment of intertia. The equations for y and I are shown in Eqs. A2 and A3 respectively.

$$\sigma = \frac{F \cdot L \cdot y}{I} \quad \text{(A1)}$$

$$y = \frac{W^2 \cdot B}{2} + \left(\frac{B^2}{4}\right) \cdot \frac{(W + B/6)}{W \cdot L + (B^2/4)} \quad \text{(A2)}$$

$$I = \frac{(B \cdot W^3)}{12} + \left(y - \frac{W}{2}\right)^2 \cdot W \cdot B + \frac{B^4}{288} + \left[\left(\frac{B^2}{4}\right) \cdot \left(\frac{W}{6}\right) + W - y\right]^2 \quad \text{(A3)}$$

With the stress at fracture calculated the plane stress linear elastic fracture toughness can be determined using Eq. A4 where σ is the stress at fracture a is the initial crack length, and f(a/W) is a geometric factor discussed in the main text and shown in Eq. 2 The elastic strain energy release rate in plane stress is related to the linear elastic fracture toughness value by Eq. A5 where E is Young's modulus.

$$K_{IC} = \sigma\sqrt{a \cdot \pi} \cdot f\left(\frac{a}{W}\right) \quad \text{(A4)}$$

$$G = \frac{{K_{IC}}^2}{E} \quad \text{(A5)}$$

As the dimensions of the micro-cantilevers are quite small a non-linear J integral approach (Eq. A6) was used to calculate the strain energy release rates for each beam where A_{curve} is the integrated area under the force-displacement curve, W is the height of the rectangular portion of the beam, a is the crack length, and B is the width of the beam. K_J is then calculated by Eq. A7 where E is elastic modulus.

$$J = \frac{2 \cdot A_{curve}}{W \cdot (B - a) + 0.25 \cdot B^2} \quad \text{(A6)}$$

$$K_J = \sqrt{J \cdot E} \quad \text{(A7)}$$

Plastic zone radius (R_y) and statistical sampling volume (SSV) were calculated using Eqs. A8 and A9 where K_{IC} is the linear elastic mode I fracture toughness, σ_y is the material yield stress (measured using nanoindentation), and E is Young's modulus.

$$SSV = \frac{K_{IC}}{\sigma_y \cdot E} \quad \text{(A8)}$$

$$R_y = \frac{1}{2\pi}\left(\frac{K_{IC}}{\sigma_y}\right)^2 \quad \text{(A9)}$$